Anomalous dynamic response of nematic platelets studied by spatially resolved rheo-small angle x-ray scattering in the 1–2 plane

Cite as: Phys. Fluids **33**, 123104 (2021); https://doi.org/10.1063/5.0069458
Submitted: 31 August 2021 • Accepted: 24 November 2021 • Published Online: 10 December 2021

O. Korculanin, F. Westermeier, H. Hirsemann, et al.

Physics of Fluids ARTICLE scitation.org/journal/phf

Anomalous dynamic response of nematic platelets studied by spatially resolved rheo-small angle x-ray scattering in the 1–2 plane

Cite as: Phys. Fluids **33**, 123104 (2021); doi: 10.1063/5.0069458
Submitted: 31 August 2021 · Accepted: 24 November 2021 ·
Published Online: 10 December 2021

O. Korculanin,[1,2] F. Westermeier,[3] H. Hirsemann,[3] B. Struth,[3] D. Hermida-Merino,[4] U. H. Wagner,[5,6] G. J. Donley,[7] S. A. Rogers,[7] and M. P. Lettinga[1,2,a)]

AFFILIATIONS

[1]Biomacromolecular Systems and Processes (IBI-4), Forschungszentrum Jülich GmbH, 52428 Jülich, Germany
[2]Laboratory for Soft Matter and Biophysics, KU Leuven, B-3001 Leuven, Belgium
[3]Deutsches Elektronen-Synchrotron DESY, Notkestr. 85, 22607 Hamburg, Germany
[4]DUBBLE CRG BM26 ESRF, Netherlands Organization for Scientific Research, 38043 Grenoble, France
[5]Diamond Light Source, Harwell Campus, Didcot OX11 0DE, United Kingdom
[6]Photon Science Division, Paul Scherrer Institut, 5232 Villigen PSI, Switzerland
[7]Department of Chemical and Biomolecular Engineering, University of Illinois at Urbana-Champaign, Champaign, Illinois 61801, USA

[a)]**Author to whom correspondence should be addressed:** p.lettinga@fz-juelich.de

ABSTRACT

Dispersions of colloidal platelets in the nematic phase display strong wall anchoring, which competes with the reorientational motion of the director when the system is subjected to flow. We show that the mechanical response to large amplitude oscillatory strain and stress depends on the confinement of the system due to this competition. We elucidate the underlying structural response by deflecting a x-ray beam vertically along the vorticity direction of a Couette geometry, such that the structure can be probed throughout the gap with an unprecedented spatial resolution while recording *in situ* the mechanical response. We observe strong inhomogeneities in terms of the orientation of the nematic director, depending on the extent of the system's yield during an oscillation. At small strain amplitudes, we observe a small region where the director oscillates between wall anchoring and the Leslie angle, while in the bulk, the director tilts out of the flow–flow gradient plane. At large strain amplitudes, the oscillations of the director are symmetric, close to the wall, and propagate into the bulk. Here, a twinning is observed where the director rotates out-of-plane in two opposite directions. Using the sequence of physical process method to analyze the LAOStrain response for both the mechanical and structural response, we locate the yielding in a small time-window around flow reversal and identify that the bulk is the main contributor to the mechanical response. The structural response to LAOStress is much less pronounced even when the stress amplitude causes significant shear thinning.

I. INTRODUCTION

Dispersions of colloidal platelets form a liquid crystalline nematic phase at sufficiently high concentrations.[1,2] Examples of such systems are clays used in the processing of many industrial materials, such as paper and ceramics. As these systems are subjected to shear flow during processing, it is of practical interest to understand their flow response. This response is complex, especially when there is orientational ordering in the nematic phase. The reason is that the director, which describes the average direction of the normal of the platelets, can undergo a tumbling motion at low shear rates, while in the flow-aligning state at higher shear rates, it exhibits an angle with the flow direction, the so-called Leslie angle.[3–8] Rheological signatures of tumbling in steady shear flow consist of a cascade of shear-thinning regions accompanied by rich behavior of the normal stresses.[9] Nonlinear behavior is also pronounced in dynamic tests, where a (double) yielding behavior can be identified.[10–12]

In situ small-angle neutron scattering (SANS)[13–15] and small-angle x-ray scattering (SAXS)[16–20] experiments, in combination with a Couette or plate-plate geometry, see Fig. 1, are most suited to quantify the orientational ordering in shear flow and thus to understand the underlying microstructural response of this rich rheological behavior. Most of these experiments are conducted such that either the flow-vorticity ($\mathbf{v} - \nabla \times \mathbf{v}$ or 1–3) or the vorticity-flow gradient ($\nabla \times \mathbf{v} - \nabla \mathbf{v}$ or 1–2) plane is probed, revealing the average orientation of the projected director in this plane as well as the degree of ordering around the projected director. For example, Dykes *et al.*[17] performed flow reversal experiments using a shear cell that was constructed such that the x-ray beam could be directed along the vorticity direction. In this way, they could nicely observe the tumbling of the director after flow reversal, although, for this system, it was not clear if it was nematic at equilibrium.

In our previous work,[19,20] we have observed a complex flow response for nematic Gibbsite subjected to large amplitude oscillatory strain (LAOStrain) and stress (LAOStress). These intrinsically non-linear dynamic experiments better reveal the rich flow response of nematic liquid crystals. It was shown that the transition from solid-like ($G' > G''$) to fluid-like ($G' < G''$) behavior with increasing strain amplitude γ_0 of the oscillations is a dynamic bifurcation at small strain amplitude due to the incomplete tilting of the platelets, while at large amplitudes the director does perform a complete rotation at flow reversal.[19] For these experiments, time-resolved SAXS was used in combination with a plate-plate geometry, probing the $\mathbf{v} - \nabla \times \mathbf{v}$ (1–3) plane of the structure. A similar transition was described in Ref. 20 for LAOStress, where oscillatory stress is applied to the system. For LAOStress, the asymmetry in the response is even more pronounced, hinting at a soft response for part of the sample. Moreover, here scattering experiments were also performed in the $\mathbf{v} - \nabla \mathbf{v}$ (1–2) plane by deflecting the x-ray beam vertically such that it could be directed along the vorticity direction of a Couette cell. Together with the plate-plate geometry data, there is full information on the reorientational motion of the director, while the mechanical response was measured simultaneously in contrast to Ref. 17.

So far, it has been assumed that the flow is homogeneous throughout the gap of a rheometer geometry. However, flow instabilities have been observed in steady shear flow connected to the tumbling motion for colloidal rods[21] and platelets.[22,23] Flow instabilities can also be caused by confinement effects. For a full understanding of sheared nematic platelets, one should consider that colloidal platelets exhibit strong wall anchoring, where the nematic director points along the normal of the wall, maximizing the free accessible volume.[24] As a result, there is a coupling between flow and director orientation, for which a complex flow behavior is predicted, where the dynamic moduli depend on the anchoring,[8,25,26] and the profile in Poiseuille flow becomes non-parabolic in terms of both structure and flow.[7,8,25,27–31] For colloidal platelets, the anchoring condition is always such that the director points along the normal of the wall, resulting in a homogeneous director field without domains.[32] Under these conditions, nematic platelets display instabilities in Poiseuille flow, see Ref. 33, but notably also under shear flow,[23] where heterogeneities in the flow, as well as the vorticity direction, were observed. In a very recent paper, we have shown that nematic Gibbsite dispersions under steady shear display instability, causing the formation of shear bands in the gradient direction, accompanied by fluctuations in the structure.[34] In these experiments, x-ray photon correlation spectroscopy (XPCS) was used, scanning the gap of a Couette cell by directing the x-ray beam along the tangent direction. This experiment provided both the dynamics as well as the static structure in the $\nabla \times \mathbf{v} - \nabla \mathbf{v}$ plane. In order to study the competition between wall anchoring and flow, experiments, where the structure is probed in the $\mathbf{v} - \nabla \mathbf{v}$ plane, are more suited as it gives access to the Leslie angle. Moreover, dynamics experiments like LAOStrain have proven to give a very rich response, which likely is much affected by confinement.

This paper investigates the relation between wall anchoring and flow of sheared nematic Gibbsite platelets, using LAOStrain and Stress to induce a non-linear response. We study the effect of confinement on the rheological response, using a plate-plate geometry for which the gap size can be varied. When the gap between the standing and moving wall of a shear cell is sufficiently wide, then it is to be expected that the wall anchoring does not propagate anymore throughout the full gap of the geometry, so that the response in the bulk of the sample, in the middle of the gap, is different from the response at the walls. We acquire space-resolved structural information by deflecting an x-ray beam vertically along the vorticity direction of a Couette geometry. By displacing the rheometer with respect to the x-ray beam, we can scan the gap of the Couette geometry in the gradient direction. In this way, we obtain structural information in the most relevant $\mathbf{v} - \nabla \mathbf{v}$ plane at a high spatial resolution, given the narrow beam waist of 40×40 μm at the P10 beam line at DESY. This is similar to previous experiments using SANS,[35,36] but the beam waist allows for a much finer spatial resolution while the fact that the x-rays can be deflected in the vertical

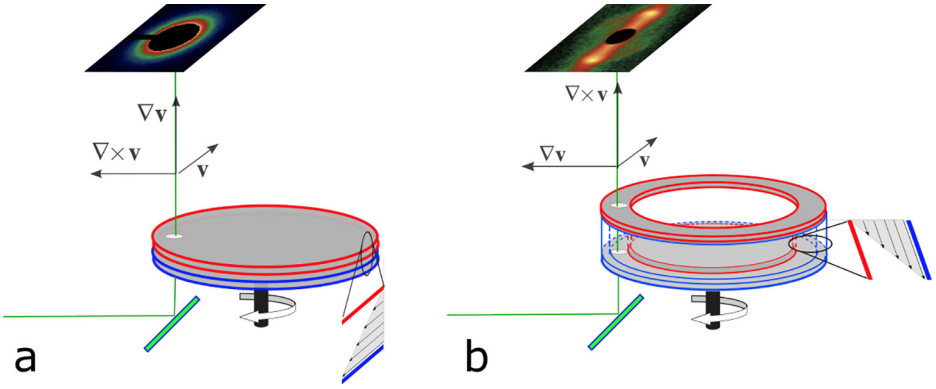

FIG. 1. Sketch of the two scattering geometries used: (a) plate–plate geometry; (b) Couette geometry. The path of the x-ray beam is indicated by the green line. We also indicate how the gap is scanned by a relative motion of the rheometer with respect to the mirror. Reproduced with permission from Korculanin *et al.* "Anomalous structural response of nematic colloidal platelets subjected to large amplitude stress oscillations," Phys. Fluids **29**, 023102 (2017). Copyright 2017 AIP Publishing.

direction allows for using a rheometer instead of a shear cell and thus for a direct comparison between mechanical and structural response. Similarly, we probe the structure *in situ* in the $\mathbf{v} - \nabla \times \mathbf{v}$ plane when using the plane–plane geometry.

The data will be analyzed by the sequence of physical process (SPP) approach, where the time-dependent storage and loss modulus and compliance are calculated from the mechanical response of the system. As such, it will prove to be a sensitive tool to identify the rheological effect of wall anchoring. Moreover, applying the SPP analysis to the high time-resolved structural data facilitates linking the structural and mechanical response, as in Ref. 37.

The paper is structured as follows: after introducing the Experiment and Analysis approach, we first present the LAOStrain response, varying the gap in the plate–plate geometry and scanning the gap in the Couette geometry. Next, we present the LAOStress response, which is much less pronounced. Finally, we discuss the results in terms of the competition between wall anchoring and flow.

II. EXPERIMENTAL

In order to correlate the micro-structural response of nematic platelets to its mechanical response, it is a prerequisite to measure both responses simultaneously. Given the turbidity of the sample and the expected nearest-neighbor correlations between platelets along the direction normal to the face of the platelets (i.e., along $\hat{n}$ of the nematic director) of the order of 50 nm, we choose small-angle x-ray scattering (SAXS) to access the micro-structural response. In our Rheo-SAXS experiments, we exploited a unique setup where the horizontal x-ray beam from a synchrotron is deflected 90° by a germanium crystal [using the (333) reflection, which corresponds to a Bragg angle of 45° at the chosen x-ray energy], such that the beam passes parallel to the rotational axis of a stress-controlled rheometer (MARS III, Thermo Fisher, Germany) used to probe the mechanical response. We used both the setup original developed by Struth *et al.*[38,39] and a mobile version.[20] The rheometer is configured such that it outputs the full response with 512 measurements per oscillation.

We used a plate–plate (diameter 20 mm) as well as a Couette geometry, both fabricated from polyimide (Vespel SP-1, DuPont) to reduce x-ray absorption and scattering at moderate x-ray energies. The Couette geometry consists of two concentric cylinders of, respectively, 30 and 28 mm, so that the gap is 1.0 mm, while the height of the cylinders is 3.0 mm, see also Ref. 39. A larger ratio between gap and height of the cell would be rheologically favorable, but a too long pathway of the beam through the sample should be avoided to minimize absorption and multiple-scattering. A 100 μm thin circle was engineered in the top part and an equally thin ring in the moving bottom part of both geometries to reduce absorption and background scattering due to the vespel, see, for example, the bright ring in Fig. 1(b). This thickness still guarantees a flat geometry, if the milling is carefully performed.

Figure 1 shows the two geometries with the respective beam direction, and the plane probed. The beam is directed along the gradient direction in the plate–plate geometry to probe the $\mathbf{v} - \nabla \times \mathbf{v}$ plane. In the Couette geometry, the beam is directed along the vorticity direction, and the $\mathbf{v} - \nabla \mathbf{v}$ plane is probed. The expected scatter patterns for three different orientations of the nematic director in the two geometries are shown in Fig. 2. In principle, the orientational distribution of ψ and ϕ is probed in the plate–plate and Couette geometry, respectively. If a sufficiently narrow beam waist is used, then we can scan the gap of the Couette geometry and probe the sample at different positions along the gradient directions.

The LAOStrain experiments with the Couette and plate–plate geometry were performed at the P10 beam line at DESY,[40] Hamburg. The beam waist for the experiments with the Couette geometry was 40 μm, which allows for high-resolution scanning of the 1.0 mm gap.

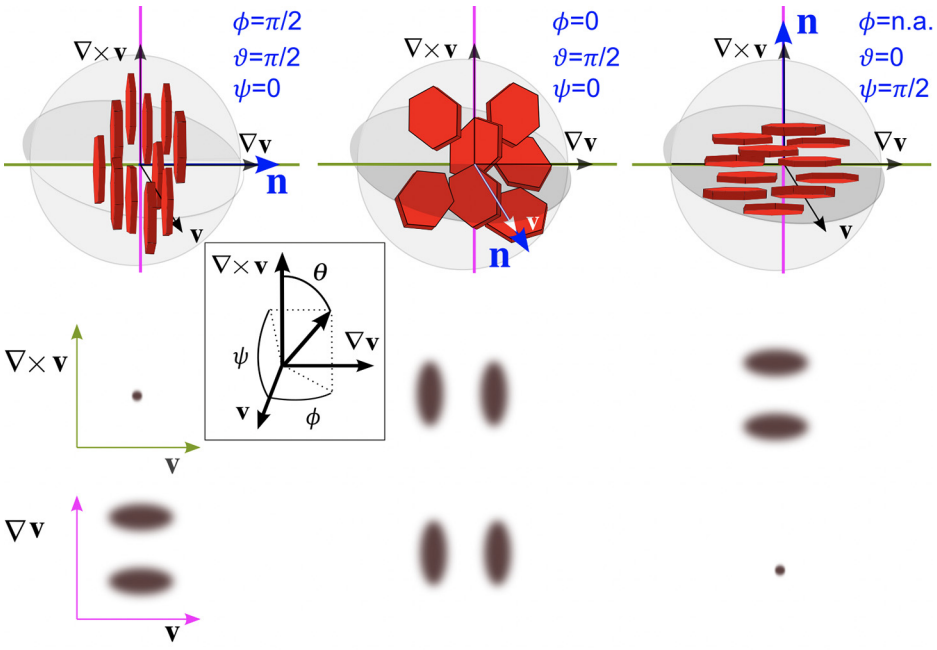

FIG. 2. Sketch of scatter patterns for three different orientations, as defined by the angles θ, ϕ and the projection in the $\mathbf{v} - \nabla \times \mathbf{v}$ plane ψ (see inset), of the nematic director **n** (top row): directing the beam along the gradient direction (green line) to probe the $\mathbf{v} - \nabla \times \mathbf{v}$ plane (middle row); directing the beam along the vorticity direction (magenta line) to probe the $\mathbf{v} - \nabla \mathbf{v}$ plane (bottom row). Reproduced with permission from Korculanin *et al.* "Anomalous structural response of nematic colloidal platelets subjected to large amplitude stress oscillations," Phys. Fluids **29**, 023102 (2017). Copyright 2017 AIP Publishing.

The plate–plate experiments were performed at a beam waste of 100 μm.[19] The LAOStress experiments with the Couette geometry were performed at the I13 beam line at Diamond,[41,42] Didcot, with a beam waist of 200×200 μm, using the same Couette geometry. Here, we could measure at the wall and in the middle of the gap. The LAOStress experiments with the plate–plate and Couette geometry were performed at the Dubble beam line ESRF,[43,44] Grenoble, with a beam waist of 400×100 μm, at different gap sizes. The photon energy for all experiments was 8.05 keV corresponding to a wavelength of $\lambda = 0.15$ nm. For detection, we used the LAMBDA detector[45,46] (55×55 μ^2 pixel size, almost 100% quantum efficiency at the used energy), at a distance of 3.5 m (DESY), 2.0 m (diamond), and 2.1 m (ESRF) downstream of the sample position. The exposure time for all experiments was 0.25 s, resulting in 100 frames per oscillation of 0.04 Hz. Scatter patterns for all three beam lines are plotted in Fig. 3(a).

All data were processed without background correction, mainly because the scattered intensity of the system under study is much higher than the background, especially in the q-range where the nematic structure peaks appears, as can be appreciated from Fig. 3(c). Of course the background also fluctuates when the geometry rotates, which can become a problem for samples with a small scattering cross section.

The colloidal platelets used in this study are synthesized in-house, following a procedure from Ref. 47. They are Gibbsite ($\gamma - Al(OH)_3$) hexagonal-shaped particles with a positively charged surface, a thickness of $L = 8.4 \pm 2.8$ nm and a diameter of $D = 250 \pm 32$ nm. The Gibbsite platelets were dispersed in water-saturated glycerol at a volume fraction of 12.7% where the suspension is in the nematic phase.

III. ANALYSIS

The mechanical response was analyzed with the sequence of physical processes (SPP) method.[37,48,49] This method views transient non-linear responses elicited from LAOS tests as being the result of a sequence of processes rather than the linear summation suggested by the mathematics of Fourier-based approaches. Within the SPP scheme, the material response is decomposed into instantaneous components. If a strain is applied, the response is stress, and the components are moduli. If stress is applied and strain is measured, the components are compliances.

The formalism of the SPP analysis is grounded in differential geometry, where a transient viscoelastic response is viewed as being caused by two orthogonal inputs. For instance, under LAOStrain, the strain and the rate are mutually orthogonal, and the measured stress is a function of both parameters. The material response is therefore a trajectory in a three-dimensional space formed by the triplet $[\gamma(t), \dot{\gamma}(t), \sigma(t)]$, where $\gamma(t)$, $\dot{\gamma}(t)$, and $\sigma(t)$ are the transient strain, strain rate, and stress, respectively. Under such conditions, we define instantaneous storage and loss moduli, G_t' and G_t'', as being the partial derivatives of the stress with respect to the strain and the strain rate

$$G_t' = \frac{\partial \sigma}{\partial \gamma}, \tag{1}$$

$$G_t'' = \frac{\partial \sigma}{\partial \dot{\gamma}}. \tag{2}$$

The analysis has been performed with a home written program. The SPP parameters have been used to create structure-property-processing relationships in colloidal[50,51] and polymeric[37] materials, in addition to our previous studies of platelets,[19,20] and has inspired new experimental methodologies.[52,53] Therefore, analyzing a transient non-linear response results in instantaneous parameters that can be compared with transient structural measures throughout the oscillation when applying large amplitude oscillatory strain.

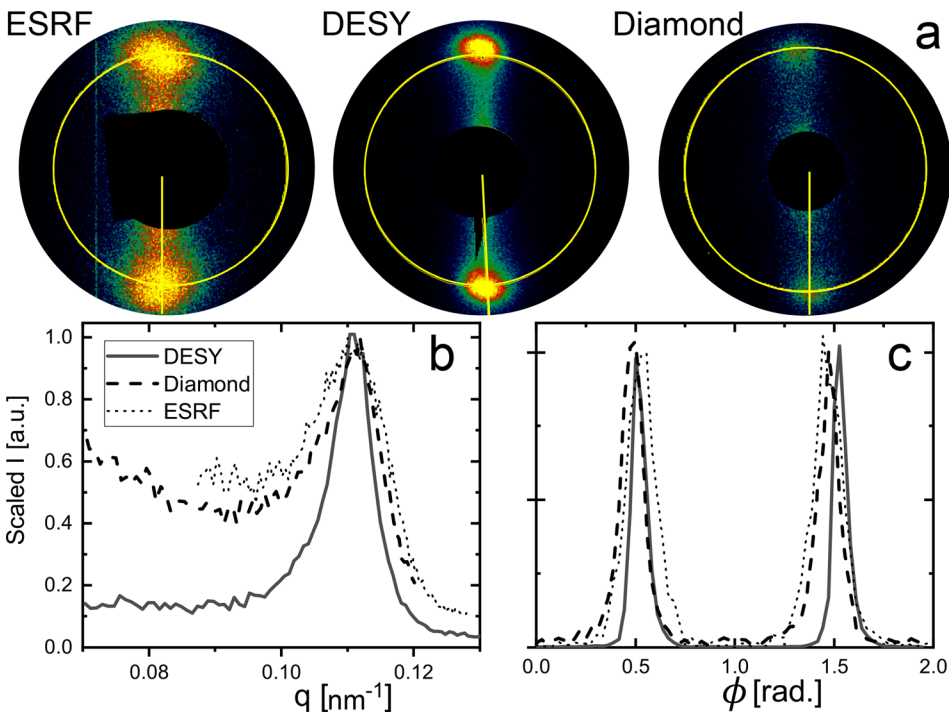

FIG. 3. (a) Scatter patterns of the nematic Gibbsite taken at ESRF, DESY, and diamond. The line indicates the angle ϕ where the radial profile was taken as plotted in (b). The circle indicates the q-vector where the azimuthal was taken, as plotted in (c).

The SPP parameters can be used to form transient Cole–Cole plots by displaying the instantaneous loss modulus vs the instantaneous storage modulus. Such presentations will be single points in space in the linear viscoelastic regime, while non-linear responses will trace out closed trajectories. Choi *et al.* showed that such plots would form deltoids when the degree of nonlinearity is small.[54] It was also shown that increasing levels of nonlinearity simply act to distort the deltoids in Cole–Cole plots. Further, Choi *et al.* showed that the time-average values of the SPP moduli are identical to the traditionally used storage and loss moduli, $G'(\omega, \gamma_0)$ and $G''(\omega, \gamma_0)$.

In two separate papers, Donley *et al.*[55,56] also used the SPP parameters to study the time-resolved nature of the yielding transition in soft materials by mapping out the rates at which the SPP parameters change. It was shown that yielding could be interpreted when a transient response changes from being predominantly elastic, where $G'_t > G''_t$, to being predominantly viscous, where $G'_t < G''_t$. This yielding transition can also be viewed in the Cole–Cole plots, as the trajectory crosses the $G'_t = G''_t$ line from below.

IV. RESULTS

A. Gap size dependence of the mechanical LAOStrain response

We first study the effect of confinement, using a plate–plate geometry for which the gap size can be varied. When the gap between the standing and moving wall of a shear cell is sufficiently wide, then it is to be expected that the wall anchoring does not propagate anymore throughout the full gap of the geometry, so that the response in the bulk of the sample, i.e., in the middle of the gap, is different than at the walls. The rheological responses for varying gap sizes are plotted in Fig. 4 at strain amplitudes of $\gamma_0 = 0.4$, 1.2, and 12.8 in rows (a)–(c), respectively. The elastic (stress vs strain) and viscous (stress vs rate) Lissajous figures are plotted in columns I–II, respectively. In this representation, non-linear behavior corresponds to a deviation from an ellipsoidal shape, which would be the linear visco-elastic response. The time-dependent Cole–Cole plots of the time-dependent storage, G'_t, vs the loss, G''_t, moduli are plotted in the right panels (column III). In this representation, non-linear behavior corresponds to the extent of excursions away from the averaged value.

At the smallest strain amplitude, the Lissajous are ellipsoidal, and the Cole–Cole plot does not show a clear dependence on the gap size and is erratic (data not shown). At $\gamma_0 = 0.4$, we observe in the Cole–Cole plot that $G''_t < G'_t$ for most of the period, which means that the system is predominantly elastic, see Fig. 4(IIIa). Indeed, the elastic Lissajous is also more stretched compared to the viscous Lissajous. However, we also identify yielding in the Cole–Cole plot, as the trajectory crosses the $G''_t = G'_t$ line when the applied deformation is approaching the strain reversal point. The responses become increasingly nonlinear for $\gamma_0 \geq 1.2$. The excursions of G''_t and G'_t become more extended and increasingly take place in a limited part of the cycle around the flow reversal, as can be appreciated from the color-coding. This hints at rapid structural changes that occur during these intervals. The data around strain reversal are condensed in the bottom corner of the $G''_t - G'_t$ deltoid, see Figs. 4(IIIb) and 4(IIIc).

We parameterize the response classically by taking the time-averaged $|G'|$ and $|G''|$ and plotting them vs the strain amplitude γ_0, see Fig. 5(a). At a strain of $\gamma_0 = 1.2$, we identify the crossover point where $|G'| = |G''|$, which is generally connected to yielding. It is, however, more insightful to parameterize the response by the instantaneous storage modulus $G'_t|_{max.}$ and the loss modulus $G''_t|_{max.}$ at the upper left corner of the deltoid where G''_t is highest, as this point undergoes the most prominent changes. $G'_t|_{max.}$ decreases continuously with increasing strain amplitude γ_0, as shown in Fig. 5(b), and crosses zero around the point where $|G'| = |G''|$. A negative value of G'_t means that the system is actually pushing the deformation instead of resisting deformation with a certain modulus, such that the system tends to recoil to its original position. Thus, there is a transition from a softening system to a recoiling system in a substantial part of the cycle.

However, this parameter does not clearly show a gap size dependence. On the contrary, $G''_t|_{max.}$ shows a broad peak for the smallest gap, which disappears with increasing gap size while shifting to low γ_0, see Fig. 5(c). This suggests that the response away from the walls, in the bulk of the material, is softer than close to the wall. To investigate this further, we scanned the gap's structure, which will be discussed in Sec. IV B. Note that the classical strain sweep in Fig. 5(a), which only accounts for average responses, does not and cannot show such apparent instantaneous differences.

B. Spatially resolved structural response to LAOStrain

To spatially resolve the structural response, we used the Couette geometry and directed the x-ray beam along the vorticity direction in order to link the mechanical response with the local structural response throughout the gap. The Couette geometry has a gap of $d = 1$ mm, which is also the largest gap we tested in the plate–plate geometry and which therefore should contain a considerable bulk contribution. Figure 6 displays the scattering patterns obtained in the $\mathbf{v} - \nabla\mathbf{v}$ plane, taken at different positions between the inner and outer wall, at flow reversal and strain reversal. Also indicated are scatter patterns taken in the $\mathbf{v} - \nabla \times \mathbf{v}$ plane using the plate–plate geometry.

The two lobes in the scatter pattern are a typical signature for the nematic phase. The peak in the radial direction defines the interparticle structure factor peak of the nearest-neighbor correlations between the platelets along the direction $\hat{n}$ of the nematic director. The location of the peak at $q_{max} = 0.11\ \mathrm{nm}^{-1}$, see Fig. 6, corresponds to a mean face-to-face distance between the platelets of 55 nm. The azimuthal profile taken at q_{max}, along the dashed line in Fig. 6, shows two peaks (as in Fig. 3(c)). The width of the peaks can be related to the orientational ordering, as discussed in Ref. 20, while the angular position of the maximum gives the orientation of the director in the probed plane, which is ϕ in the $\mathbf{v} - \nabla\mathbf{v}$ plane and ψ in the $\mathbf{v} - \nabla \times \mathbf{v}$ plane, see Fig. 2 (top). The angles can be determined with a high precision of $\approx$0.001 Rad. The absolute intensity is indicative of the director's tilt out of the scattering plane toward the probing beam. If it points along the probing beam, then the structure peak disappears, as schematically shown in Fig. 2 (bottom). The time- and space-resolved structural responses are generally very heterogeneous. As it turned out, structural changes are mainly due to the reorientation of the director, and therefore, we use in the following mostly ϕ but also the intensity to quantify the structural response.

At the *smallest applied strain amplitude* of $\gamma_0 = 0.4$, the angle ϕ and the intensity oscillate slightly close to the moving wall (0.05 mm from the wall) and almost not in the middle, where the intensity is significantly lower, see Figs. 7(aI) and 7(bI). The response close to the wall is not symmetric, as the director oscillates between the equilibrium wall anchoring position of $\phi = 0.500$ and $\phi = 0.506\pi$, which

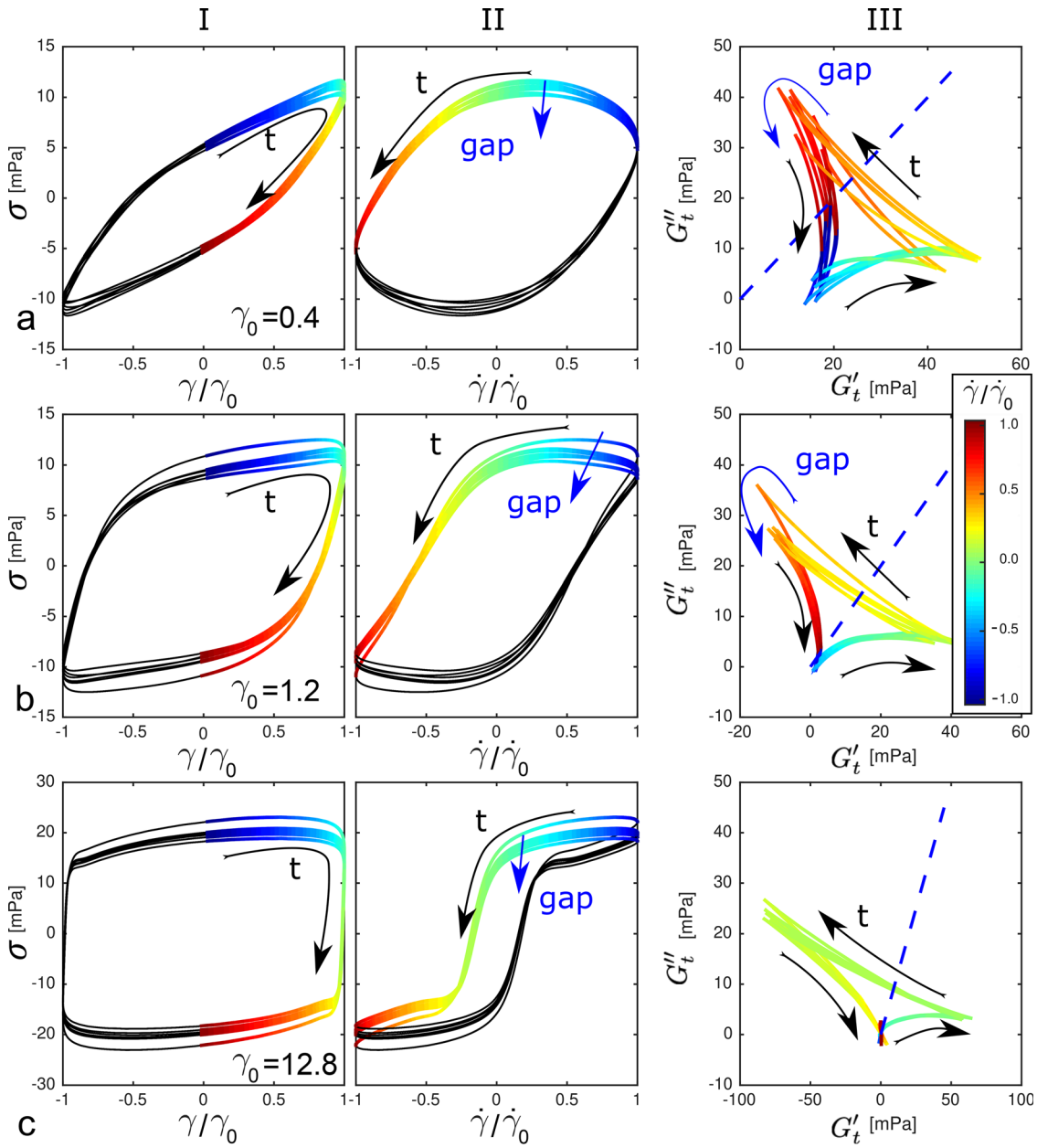

FIG. 4. Large amplitude oscillatory shear (LAOStrain) responses and associated material physics for strain amplitudes of [row (a)] $\gamma_0 = 0.4$, [row (b)] $\gamma_0 = 1.2$ and [row (c)] $\gamma_0 = 12.8$ at different gap sizes. Elastic Lissajous curves of shear stress vs shear strain (column I) and viscous Lissajous curves of shear stress vs shear rate (column II). In this representation, non-linear behavior corresponds to a deviation from an ellipsoidal shape, which would be the linear visco-elastic response. Column III: Cole–Cole plot of the time-dependent G'_t vs G''_t. A yielding from a solid ($G'_t > G''_t$) to a fluid response ($G'_t < G''_t$) takes place when the trajectory crosses the line $G'_t = G''_t$ (dashed line). The color coding in the trajectories represents the instantaneous scaled shear rate during the cycle, where the arrow indicates the direction. The blue arrow indicates increasing gap size between 0.3 and 1.0 mm.

corresponds to the Leslie angle at that shear rate. This means that the nematic director is being tilted away from the anchoring position for half of the period, and for the other half, it is bound to the anchoring position. The response is also heterogeneous throughout the gap, as the intensity of the structure factor peak rapidly decreases up to a fifth of the gap, after which it recovers toward the standing wall, see Fig. 8(b). This means that the director tilts out of the $\mathbf{v} - \nabla\mathbf{v}$ plane in the bulk of the material.

With this result, we can attribute the anomalous first harmonic response of the rotation in the $\mathbf{v} - \nabla \times \mathbf{v}$ plane, which was described

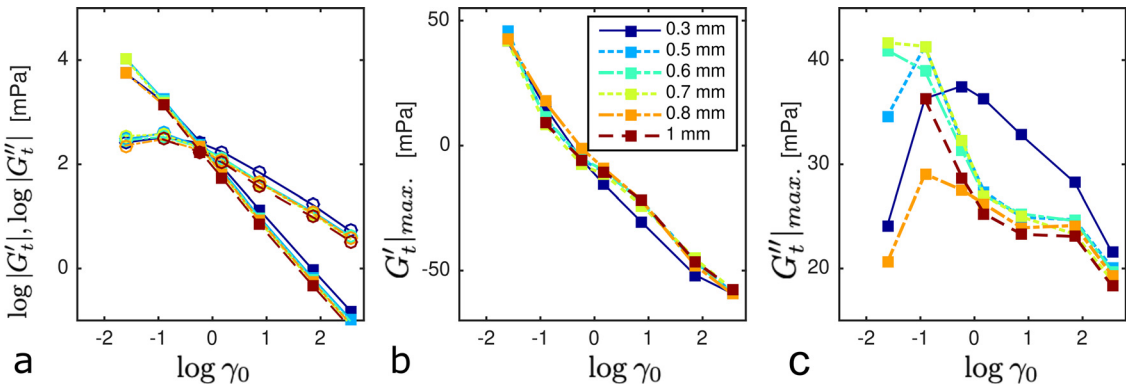

FIG. 5. (a) The time-averaged $|G'|$ (solid squares) and $|G''|$ (circles) vs the strain amplitude. (b) $G'_t|_{max.}$ and (c) $G''_t|_{max.}$ vs strain amplitude, taken at the maximum in G''_t of the mechanical property deltoids.

earlier for small strain amplitudes in Ref. 19, to the response of the director in the bulk. Indeed, the director should be tilted out of the $\mathbf{v} - \nabla\mathbf{v}$ plane for the structure to become visible in the $\mathbf{v} - \nabla \times \mathbf{v}$ plane. Close to the wall, the wall anchoring prevails, which forces the director in the $\mathbf{v} - \nabla\mathbf{v}$ plane.

To identify the correlation between the structural and mechanical responses to LAOStrain, we plot ϕ vs G'_t and G''_t in Figs. 7(aII) and 7(aIII). Clearly, the transition between the wall anchoring and Leslie angle takes place at the moment of flow reversal, where also G'_t and G''_t change rapidly. Hence, the mechanical response is correlated with the structural response at the wall, though we know that in the bulk, a rotation takes place out of the $\mathbf{v} - \nabla\mathbf{v}$ plane.

At the *largest applied strain amplitude* of $\gamma_0 = 12.8$, we observe clear oscillatory traces of the director in terms of ϕ close to the wall (at 0.05 mm from the moving wall), see Fig. 7(cI). The oscillations are symmetric around the gradient direction ($\phi = 0.5\pi$) with an amplitude of $\Delta\phi_d = 0.04\pi$. This angle can be interpreted as the typical Leslie angle of the director with respect to the flow direction.

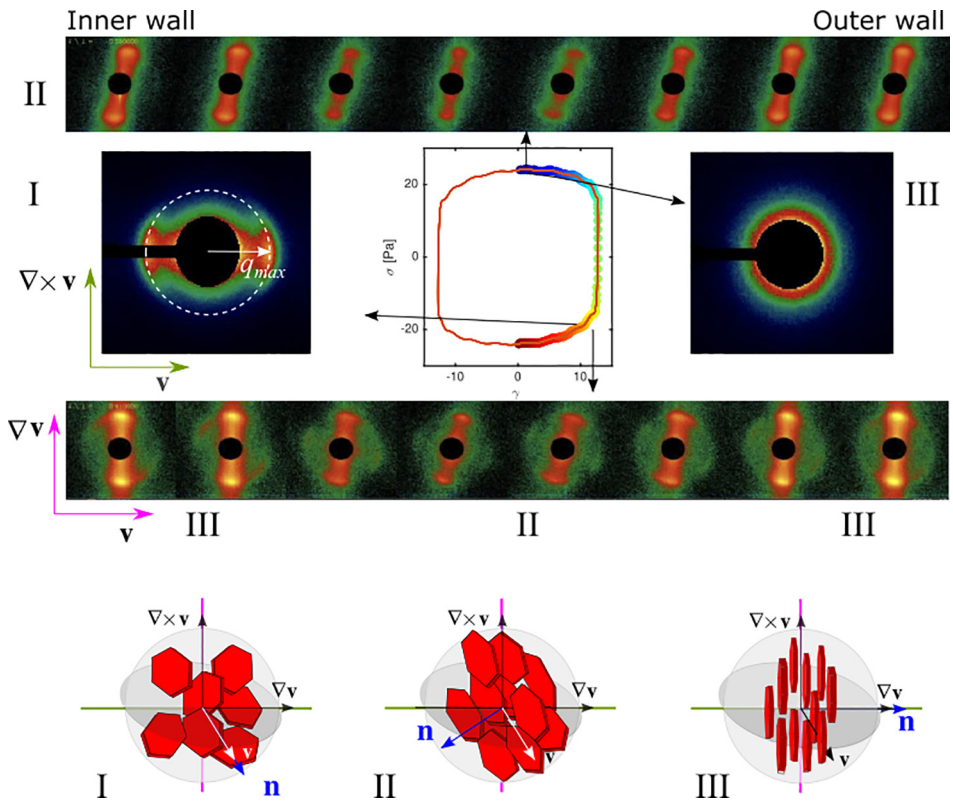

FIG. 6. SAXS patterns in the $\mathbf{v} - \nabla\mathbf{v}$ plane, throughout the gap with an interval of 100 μm, and in the $\mathbf{v} - \nabla \times \mathbf{v}$ plane. The patterns were taken at two points in the cycle as indicated in the Lissajous curve, for $\gamma_0 = 12.8$. The colored symbols in the Lissajous curve indicate the average response while the color coding represents time in the cycle. In the bottom row, we indicate a cartoon of the platelet orientation associated with the observed scatter patterns, as indicated by the roman numbers. The data were taken at DESY at two separate beam times using different beam stops. The patterns in the $\mathbf{v} - \nabla\mathbf{v}$ plane are plotted on a log scale. Multimedia view: https://doi.org/10.1063/5.0069458.1

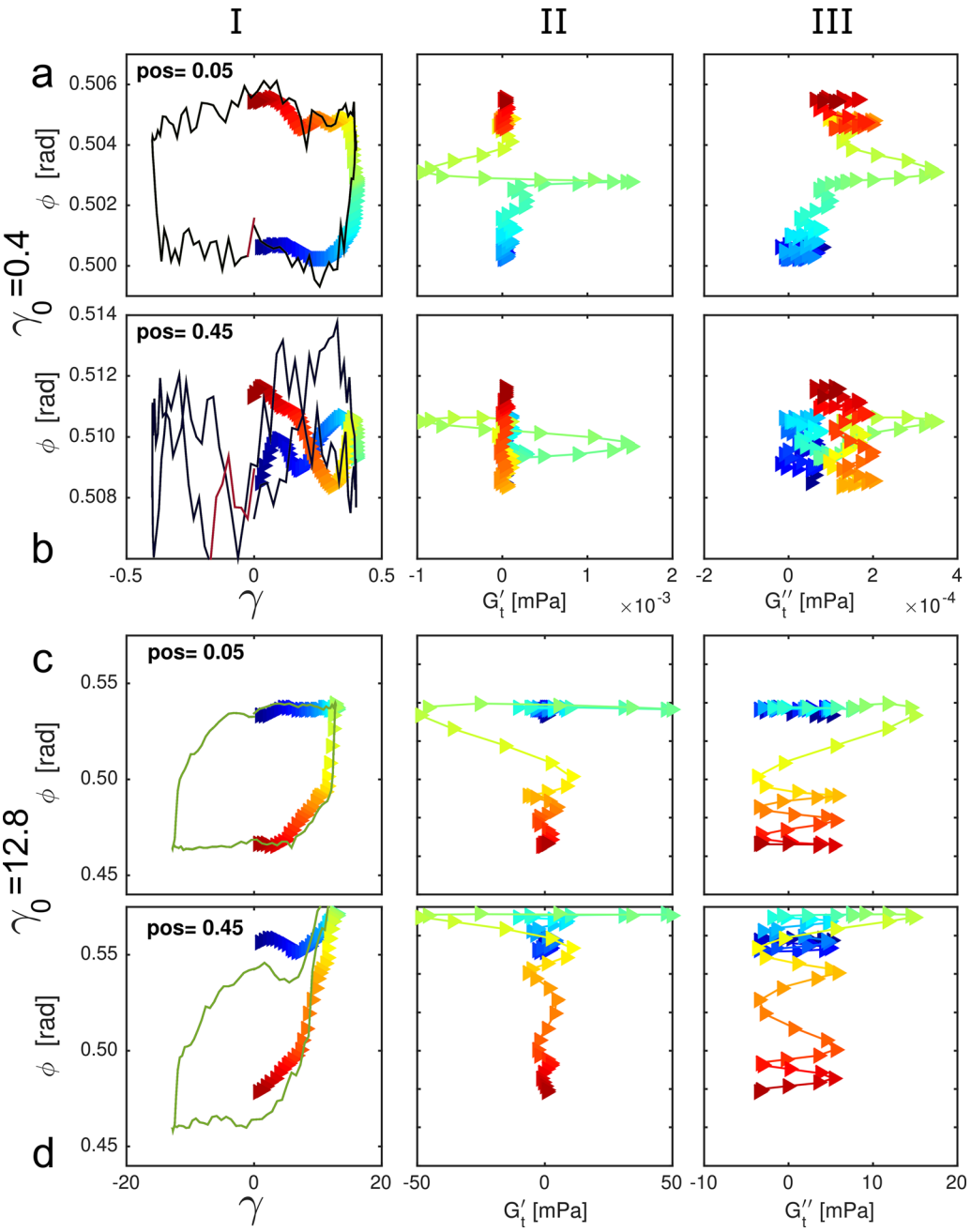

FIG. 7. Structural response of the angle ϕ to LAOStrain for two strain amplitudes: $\gamma_0 = 0.4$ [row (a) and (b)] and $\gamma_0 = 12.8$ [row (c) and (d)], taken close to the wall [row (a) and (c)] and in the middle of the gap [row (b) and (d)]. ϕ is plotted against strain γ (column I), the time-resolved storage modulus G_t' (column II), and loss modulus G_t'' (column III). The symbols indicate the average response, while their color coding represents the instantaneous scaled shear rate during the cycle, see also Fig. 4. The lines in the left column represent the response throughout one exemplary cycle.

The trajectory is in itself non-linear as the curve displays a block-like function.

The response in the middle of the cell, Fig. 7(dI), is very different, showing a bifurcation. For half of the period, roughly for the duration when the applied strain is negative, the director in the middle behaves like the director at the wall: $\Delta\phi_d \approx 0.046\pi$ and the intensity is high, see Fig. 8(a). However, the response becomes markedly different when the director tilts toward $\Delta\phi_d \to 0.054\pi$, that is, where the shear rate is highest. The intensity drops while substantial and irregular excursions in ϕ_d are observed. The intensity is at its minimum around the flow

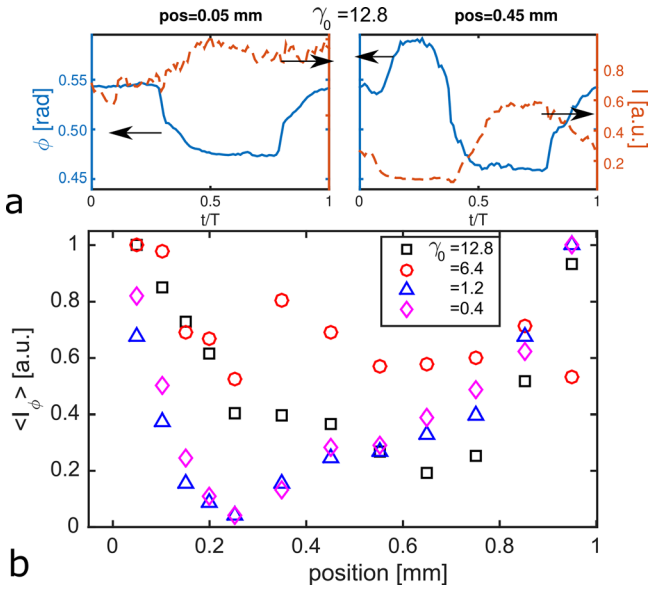

FIG. 8. (a) Typical traces of (a) the angle ϕ (blue, solid) and the maximum intensity at the peak (orange, dashed) at two positions in the gap for the largest applied strain amplitude. (b) The averaged intensity $\langle I_\phi \rangle$ vs the gap position for the indicated γ_0.

reversal (i.e., maximum strain), as can also be seen in Fig. 8(a), where angle and intensity are plotted vs time.

In our earlier work,[19,20] we observed a flash of scattering in the $\mathbf{v} - \nabla \times \mathbf{v}$ plane around flow reversal, which is only possible when the director is oriented in the vorticity direction. Thus, we can conclude that for half of the oscillation, the director loses the alignment imposed by the wall and drifts toward the vorticity direction, though less dramatically compared to small strain amplitudes so that the main projection of the director is still in the $\mathbf{v} - \nabla\mathbf{v}$ plane.

We link this behavior to an important feature observed throughout the gap: at flow reversal, when the director tilts back, a low-intensity peak splits from the main scattering peak and undergoes a full rotation in the opposite direction of the main peak. The intensity of this contribution is low, which indicates that the director is rotating out of the $\mathbf{v} - \nabla\mathbf{v}$ plane into the $\mathbf{v} - \nabla \times \mathbf{v}$ plane, causing the observed "flashes." Thus, the structure displays a twinning behavior, where part of the sample undergoes a counter-rotation relative to the rest of the sample. It also means that the sample is inhomogeneous in the vorticity direction as both types of trajectories are detected, while the beam is directed through the vorticity direction, thus sampling all responses in that direction. Indeed, inhomogeneities in the vorticity direction have also been identified for nematic graphene oxide[23] where this type of reorientational motion is caused by vortex flow. The transition between both types of behavior, at small and large γ_0, can be identified at a strain amplitude between $\gamma = 1.2$ and $\gamma = 2.4$, so around the crossover $|G'| = |G''|$.

The correlation between the structural and mechanical response to LAOStrain is established in Figs. 7(cII) and 7(cIII), showing that both the Leslie angles for the positive and negative shear rate are connected by the changes in the SPP parameters, G'_t as well as G''_t, where initially ϕ remains constant, and it only changes in the last part of the excursion, as indicated by the color-coding. Thus, the system has to recoil before the angle can change.

To better access the temporal relation between mechanical and structural responses, we performed the SPP analysis also for instantaneous contributions to the angular trace that are in-phase with the strain, ϕ'_t, and the strain-rate, ϕ''_t, replacing the stress trace by the angle trace in Eqs. (1) and (2). The time-dependent Cole–Cole plots for the mechanical and structural response are displayed in Figs. 9(a) and 9(b), respectively. Each branch of the mechanical deltoid is given a color, identifying three time intervals, which are then used for the structural Cole–Cole plot. This plot shows that nothing changes in the structural response, while the elastic modulus increases. The increase in ϕ'_t sets in at the same moment when the elastic modulus starts to decrease at the lower right corner of the deltoid. This is the instant of flow reversal, as indicated by the open symbol. Likewise, ϕ'_t starts to decrease at the next corner of the deltoid at the maximum mechanical recoil. Finally, the structure relaxes to the origin, while the mechanical modulus is at its minimum. Thus, we conclude that the structural response is enslaved by the mechanical response and lags behind. This cycle takes place in a small time interval around the flow reversal, as can be appreciated from the color-coded symbols in Figs. 9(c) and 9(d), which exactly correspond to the selected time interval in Figs. 9(a) and 9(b).

The structural response in the middle of the gap is too erratic to perform the SPP analysis. The spikes in the response, as displayed in Fig. 7(dI), are exemplary but could probably equally well be found at the maximum negative strain. It shows that the response in the middle of the gap is less dominated by the wall anchoring, which puts a constraint on the orientation of the platelets. We conclude that the elastic modulus increases toward flow reversal and that a true structural yielding takes place at flow reversal, causing a dramatic rotation of the director, especially at the wall. In the middle of the gap, the erratic changes will smooth the mechanical response. The erratic out-of-plane rotations in the middle of the gap also cause the dip in the profile of $\langle I_\phi \rangle$, see Fig. 8(b), but the dip is less pronounced as compared to the small strain amplitude, so that one can conclude that the shear propagates throughout the full gap.

C. Gap size dependence of the mechanical and structural LAOStress response

A fundamental difference between strain- and stress-controlled experiments is that the deformation of the system is always enforced in strain-controlled experiments. In contrast, in the case of stress-controlled experiments, the system "decides" whether the applied stress is high enough to deform. Figure 10 shows the LAOStress responses and associated material physics for varying stress amplitudes σ_0 at a gap of 0.5 mm in the plate–plate geometry. The strain response becomes predominantly viscous-like with increasing stress amplitudes σ_0 as it evolves to a linear dependence between strain and stress rate.

In order to investigate the effect of the gap size, we parameterize the Cole–Cole deltoid again now by identifying $J'_t|_{max.}$ and $J''_t|_{max.}$ at the upper left corner of the deltoid. The results are plotted as a function of σ_0 for two gap sizes in Fig. 11. Two conclusions can be drawn. First, $J'_t|_{max.}$ displays a distinct decrease and $J''_t|_{max.}$ a distinct increase above a critical stress amplitude. Interestingly, however, this yielding takes place earlier for the wider gap. This further suggests that the

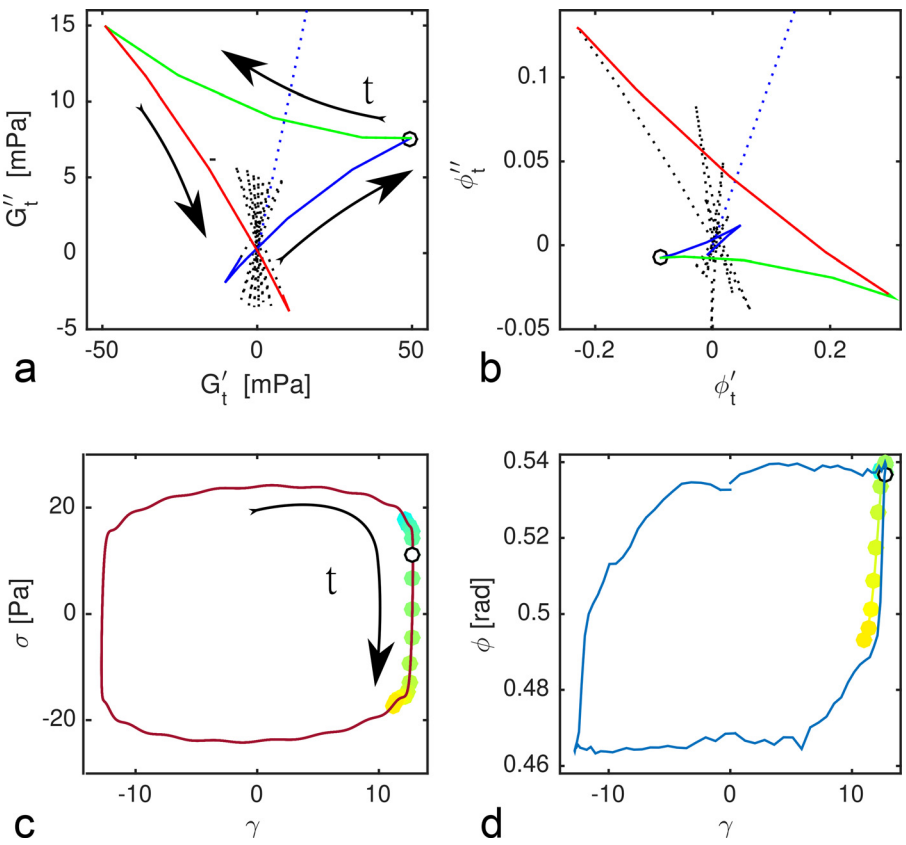

FIG. 9. Cole–Cole plot of the time-dependent (a) G_t' vs G_t'', where the dashed line marks $G' = G''$, and (b) ϕ_t' vs ϕ_t'' for a strain amplitude of $\gamma_0 = 12.8$ where the structural data are taken close to the wall (position = 0.05 mm). Here, the dashed line marks $\phi' = \phi''$. The color coding is assigned according to the three branches of the structural response. This plot suggests that structural response is enslaved by the mechanical response. (c) and (d) The corresponding Lissajous plots where the dots indicate the time window of the identified branches in (a). The flow reversal point is indicated by the open symbol.

yielding takes place in the bulk of the system, which is more susceptible to deformation and hence "softer."

The major difference with LAOStrain is that no reorientational motion is observed in the $\mathbf{v} - \nabla \times \mathbf{v}$ plane at low-stress amplitude. Only when the structure yields, occasional flashes can be observed in the $\mathbf{v} - \nabla \times \mathbf{v}$ plane similar to the large strain amplitudes. This suggests that wall anchoring is valid throughout the full gap (data not shown). To obtain a better view of this process, we also performed LAOStress with the Couette geometry, where the gap is fixed, thus probing the structure in the $\mathbf{v} - \nabla \mathbf{v}$ plane. Up to the yielding point at $\sigma_0 = 5$ Pa, which is a factor of two higher than for the plate–plate geometry for experimental reasons, the response is very noisy (data

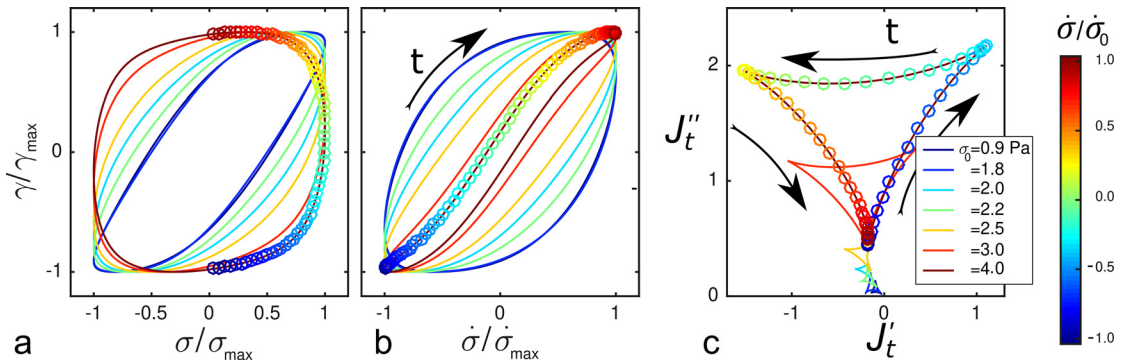

FIG. 10. Large amplitude oscillatory stress (LAOStress) responses and associated material physics for varying stress amplitudes σ_0 at a gap of 0.5 mm. (a) Elastic Lissajous curve of shear strain vs shear stress and (b) viscous Lissajous curve of shear strain vs shear stress rate, all scaled by their maximum. (c) Cole–Cole plot of the time-dependent J_t' vs J_t''. The symbols indicate the average response, while their color coding represents the instantaneous scaled stress rate during the cycle, as indicated by the color bar.

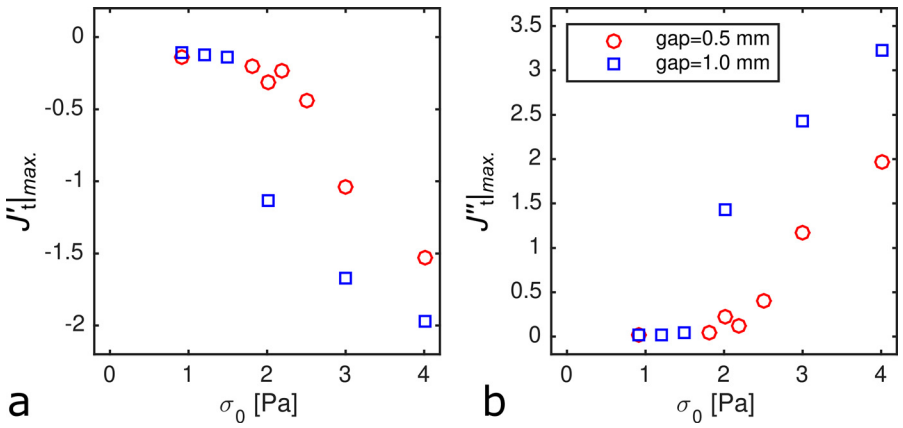

FIG. 11. $J'_t|_{max.}$ (a) and $J''_t|_{max.}$ (b) vs stress amplitude, taken at the upper left corner of the deltoid, see Fig. 10(c), for two gap sizes.

not shown). For $\sigma_0 = 8.0$ and 12 Pa, we do observe a clear structural response, see Fig. 12. For $\sigma_0 = 8.0$, the response at the wall and in the middle is very similar, while for $\sigma_0 = 12$ Pa, the amplitude in the stress is somewhat more pronounced and a clear difference between the response in the bulk and at the wall can be observed, hinting to a smaller influence of wall anchoring.

V. DISCUSSION

This paper investigates the competition between wall anchoring and flow of sheared colloidal platelets in the nematic phase, by applying large amplitude oscillatory stress and strain and studying the homogeneity in the structural response throughout the gap. Previous dynamic strain sweep tests showed that the system yields at a strain of around $\gamma_0 = 1$,[19] much higher than reported for other, more charged, platelets.[11] It was suggested that wall anchoring plays an important role in the response.

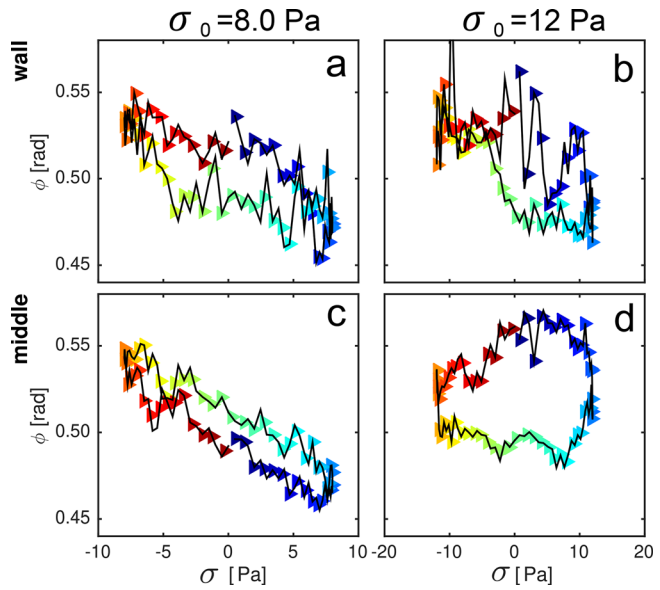

FIG. 12. Structural response vs applied stress for $\sigma_0 = 8$ (a) and (c) and 12 Pa (b) and (d), close to the wall (a) and (b) and in the middle of the Couette cell (c) and (d). The symbols indicate the average response, while their color coding represents the instantaneous scaled stress rate during the cycle, see Fig. 10. Data were taken at diamond.

The SPP analysis we employed shows that the yielding of the system takes place in a very limited part of the cycle around flow reversal and that the effect of confinement is apparent in the $G'_t - G''_t$ Cole–Cole plot where there is maximum recoil, when $G'_t \ll 0$ and G''_t reaches its maximum. As $G''_t|_{max.}$ at this point is higher for small gap sizes; this suggests that the response in the bulk of the material is softer than close to the wall. Indeed, the structural gap scan shows that twinning and out-of-plane reorientational motion takes place in bulk, reducing the stress. This motion is suppressed close to the wall due to the wall anchoring, as can be inferred from the high intensity of the structure peaks close to the walls. Applying the SPP analysis to the angle of the director, we infer that the reorientational motion of the director close to the wall is enslaved by the recoil, which takes place before the reorientation and which could find its origin in the out-of-plane motion in bulk. These observations of the spatially resolved structure therefore form the structural underpinning of the lower moduli measured for larger gaps. Our results confirm the predicted dependence of the loss and storage moduli on the anchoring condition by Choate *et al.*[26] However, in this theory rods are considered for which the nematic director has a degenerated orientation at the wall, whereas, for platelets, the director homogeneously points along the normal of the wall. Therefore, a similar theory that describes the sequences of processes would be needed for this very relevant system.

Our results are also in line with several earlier experimental which showed that the boundary wall effects are predominant at small shear rates. Similar to our results, SAXS scans on thermotropic nematic rods in Poiseuille flow[57] revealed a decay in orientation from the wall inward. Wall anchoring, in terms of lamella oriented with their normal parallel to the surface normal, was also observed for thermotropic rods in the lamellar phase,[58] and high aspect-ratio platelets.[59] For both systems, the orientation becomes unstable at high shear rates, which is also the case for graphene oxide sheets.[23] These instabilities are likely caused by the coupling between thermal fluctuations of the lamellar structures with the induced flow. This is not the case for the relatively low aspect ratio Gibbsite particles, so that one would expect that anchoring is more stable for low aspect ratio platelets. However, wall anchoring is expected to be stronger for high aspect ratio platelets,

while also the Leslie angle will decrease, which would favor a more homogeneous response.

Our observation indicates that lower aspect ratio platelets do display flow instabilities, as was also observed for mineral clays.[18] The steep decrease in intensity at $\gamma_0 = 0.4$ suggests that wall slip could occur at lower shear rates, while the inhomogeneity in the intensity at $\gamma_0 = 12.8$ suggests shear banding at high shear rates, both of which were observed in Ref. 34. However, it should be noted that LAOStrain provokes more dramatic structural responses than observed for steady shear flow due to the flow reversal. Moreover, as predicted by Klapp and Hess,[60] the response is very different when controlling the stress, leading to less structural changes. It has to be mentioned here, though, that the rheo-SAXS experiments with LAOStress measurements were performed with a lower spatial resolution.

In addition to the insights into the flow response of the nematic platelets, our experiments are also exemplary for the strength of the technique that we used. As the $\mathbf{v} - \nabla\mathbf{v}$ plane is the most relevant plane to probe, earlier efforts have been made to probe this plane and scan the gap for other systems using SANS.[35,36] The drawback of that technique is that there are no SANS beam lines available where neutrons are deflected in the vertical direction, such that, in order to probe the $\mathbf{v} - \nabla\mathbf{v}$ plane, shear cells are used where the rotational axis is horizontal. Consequently, no *in situ* rheology can be performed, and no stress-controlled measurements can be carried out, which provide useful information that is complementary to the strain-controlled data and helps us to better understand the underlying physics. Moreover, the low flux of neutrons does not allow for a high spatial resolution in a reasonable experimental time. Gap scans were also performed earlier with SAXS,[18] but in this case, the beam was directed along the flow direction, which again is not the optimal direction for this system. The $\mathbf{v} - \nabla\mathbf{v}$ plane has been probed in Ref. 33 in pipe flow. Though these geometries have the advantage that they can be easily used for wide-angle x-ray scattering (WAXS),[61] which is limited for our setup, again no *in situ* rheology is feasible with this scheme as is the case with the method we present here.

VI. CONCLUSION

Our results for nematic colloidal platelets subjected to LAOStrain show a pronounced gap dependence that can be attributed to the wall anchoring of the platelets, as we found by scanning the gap with a narrow, deflected, x-ray beam pointing along the vorticity direction of a Couette cell. A strong non-linear behavior with abrupt yielding at flow reversal is observed, which results in an in-plane tilt close to the wall and twinning of structure and out of plane tilting in the bulk. Stress-controlled experiments show a much smoother and more gradual response. The observed structural inhomogeneities suggest that the velocity profile might be non-linear, as some of us recently showed steady shear flow using x-ray photon correlation spectroscopy.[34] These findings are very relevant in view of using clay as flow modifiers in industrial systems, but also when processing other platelet particles, such as graphene oxide.[62] Moreover, we can take inspiration from these results when interpreting the flow of other yielding fluids.

ACKNOWLEDGMENTS

O.K. acknowledges the International Helmholtz Research School of Biophysics and Soft Matter for financial support.

S.A.R. and G.J.D. acknowledge support from NSF Grant No. 1847389 and the Laboratory Directed Research and Development program at Sandia National Laboratories. Sandia National Laboratories is a multimission laboratory managed and operated by National Technology and Engineering Solutions of Sandia LLC, a wholly owned subsidiary of Honeywell International Inc. for the U.S. Department of Energy's National Nuclear Security Administration Contract No. DE-NA0003525.

We acknowledge Diamond Light Source for providing beam time under the Proposal No. MT4998-1.

AUTHOR DECLARATIONS

Conflict of Interest

The authors have no conflicts to disclose.

DATA AVAILABILITY

The data that support the findings of this study are available from the corresponding author upon reasonable request.

REFERENCES

[1]F. M. van der Kooij, A. P. Philipse, and J. K. G. Dhont, "Sedimentation and diffusion in suspensions of sterically stabilized colloidal platelets," Langmuir **16**, 5317–5323 (2000).
[2]J. A. C. Veerman and D. Frenkel, "Phase behavior of disklike hard-core mesogens," Phys. Rev. A **45**, 5632–5648 (1992).
[3]F. Leslie, "Some constitutive equations for liquid crystals," Arch. Rational Mech. Anal. **28**, 265–283 (1968).
[4]T. Carlsson, "The possibility of the existence of a positive leslie viscosity α_2. Proposed flow behavior of disk like nematic liquid crystals," Mol. Cryst. Liquid Cryst. **89**, 57–66 (1982).
[5]T. Yamamoto, T. Suga, and N. Mori, "Brownian dynamics simulation of orientational behavior, flow-induced structure, and rheological properties of a suspension of oblate spheroid particles under simple shear," Phys. Rev. E **72**, 021509 (2005).
[6]A. P. Singh and A. D. Rey, "Effect of long-range elasticity and boundary conditions on microstructural response of sheared discotic mesophases," J. Non-Newtonian Fluid Mech. **94**, 87–111 (2000).
[7]D. Grecov and A. D. Rey, "Theoretical and computational rheology for discotic nematic liquid crystals," Mol. Cryst. Liquid Cryst. **391**, 57–94 (2003).
[8]D. Grecov and A. D. Rey, "Transient rheology of discotic mesophases," Rheol. Acta **42**, 590–604 (2003).
[9]M. Moan, T. Aubry, and F. Bossard, "Nonlinear behavior of very concentrated suspensions of plate-like kaolin particles in shear flow," J. Rheol. **47**, 1493 (2003).
[10]I. Arief and P. Mukhopadhyay, "Two-step yielding in novel CoNi nanoplatelet-based magnetic fluids under oscillatory rheology," Mater. Lett. **167**, 192–196 (2016).
[11]F. Bossard, M. Moan, and T. Aubry, "Linear and nonlinear viscoelastic behavior of very concentrated plate-like kaolin suspensions," J. Rheol. **51**, 1253 (2007).
[12]S. Jogun and C. F. Zukoski, "Rheology of dense suspensions of platelike particles," J. Rheol. **40**, 1211–1232 (1996).
[13]H. J. M. Hanley, G. C. Straty, and F. Tsvetkov, "A small angle neutron scattering study of a clay suspension under shear," Langmuir **10**, 3362–3364 (1994).
[14]B. Hammouda, J. Mang, and S. Kumar, "Shear-induced orientational effects in discotic-liquid-crystal micelles," Phys. Rev. E **51**, 6282–6285 (1995).
[15]A. B. D. Brown and A. R. Rennie, "Monodisperse colloidal plates under shear," Phys. Rev. E **62**, 851–862 (2000).
[16]S. M. Jogun and C. F. Zukoski, "Rheology and microstructure of dense suspensions of plate-shaped colloidal particles," J. Rheol. **43**, 847–871 (1999).
[17]L. M. Dykes, J. M. Torkelson, W. R. Burghardt, and R. Krishnamoorti, "Shear-induced orientation in polymer/clay dispersions via *in situ* x-ray scattering," Polymer **51**, 4916–4927 (2010).

[18]A. M. Philippe, C. Baravian, M. Jenny, F. Meneau, and L. J. Michot, "Taylor-Couette instability in anisotropic clay suspensions measured using small-angle x-ray scattering," Phys. Rev. Lett. **108**, 254501 (2012).
[19]M. P. Lettinga, P. Holmqvist, P. Ballesta, S. Rogers, D. Kleshchanok, and B. Struth, "Nonlinear behavior of nematic platelet dispersions in shear flow," Phys. Rev. Lett. **109**, 246001 (2012).
[20]O. Korculanin, D. Hermida-Merino, H. Hirsemann, B. Struth, S. A. Rogers, and M. P. Lettinga, "Anomalous structural response of nematic colloidal platelets subjected to large amplitude stress oscillations," Phys. Fluids **29**, 023102 (2017).
[21]M. P. Lettinga, Z. Dogic, H. Wang, and J. Vermant, "flow behavior of colloidal rodlike viruses in the nematic phase," Langmuir **21**, 8048–8057 (2005).
[22]A. B. D. Brown and A. R. Rennie, "Images of shear-induced phase separation in a dispersion of hard nanoscale discs," Chem. Eng. Sci. **56**, 2999–3004 (2001).
[23]J. K. Wychowaniec, M. Iliut, B. Borek, C. Muryn, O. O. Mykhaylyk, S. Edmondson, and A. Vijayaraghavan, "Elastic flow instabilities and macroscopic textures in graphene oxide lyotropic liquid crystals," npj 2D Mater. Appl. **5**, 11 (2021).
[24]L. Harnau and S. Dietrich, "Fluids of platelike particles near a hard wall," Phys. Rev. E **65**, 021505 (2002).
[25]E. P. Choate, M. G. Forest, and L. Ju, "Effects of strong anchoring on the dynamic moduli of heterogeneous nematic polymers II: Oblique anchoring angles," Rheol. Acta **49**, 335–347 (2010).
[26]E. P. Choate and M. G. Forest, "Dependence of the dynamic moduli of heterogeneous nematic polymers on planar anchoring relative to flow direction," Rheol. Acta **50**, 767–778 (2011).
[27]S. Heidenreich, S. Hess, and S. H. L. Klapp, "Shear-induced dynamic polarization and mesoscopic structure in suspensions of polar nanorods," Phys. Rev. Lett. **102**, 028301 (2009).
[28]V. M. O. Batista, M. L. Blow, and M. M. Telo da Gama, "The effect of anchoring on the nematic flow in channels," Soft Matter **11**, 4674–4685 (2015).
[29]T. Börzsönyi, Á. Buka, A. P. Krekhov, and L. Kramer, "Response of a homeotropic nematic liquid crystal to rectilinear oscillatory shear," Phys. Rev. E **58**, 7419–7427 (1998).
[30]C. J. Holmes, S. L. Cornford, and J. R. Sambles, "Small surface pretilt strikingly affects the director profile during Poiseuille flow of a nematic liquid crystal," Phys. Rev. Lett. **104**, 248301 (2010).
[31]A. Sengupta, S. Herminghaus, and C. Bahr, "Opto-fluidic velocimetry using liquid crystal microfluidics," Appl. Phys. Lett. **101**, 164101 (2012).
[32]A. Verhoeff, R. Brand, and H. Lekkerkerker, "Tuning the birefringence of the nematic phase in suspensions of colloidal gibbsite platelets," Mol. Phys. **109**, 1363–1371 (2011).
[33]S. Barè, J. K. Cockcroft, S. L. Colston, A. C. Jupe, and A. R. Rennie, "X-ray study of the orientational order of a concentrated dispersion of kaolinite under flow," J. Appl. Crystallogr. **34**, 573–579 (2001).
[34]Y. Chen, O. Korculanin, S. Narayanan, J. Buitenhuis, S. A. Rogers, R. L. Leheny, and M. P. Lettinga, "Probing nonlinear velocity profiles of shear-thinning, nematic platelet dispersions in Couette flow using x-ray photon correlation spectroscopy," Phys. Fluids **33**, 063102 (2021).
[35]M. W. Liberatore, F. Nettesheim, P. A. Vasquez, M. E. Helgeson, N. J. Wagner, E. W. Kaler, L. P. Cook, L. Porcar, and Y. T. Hu, "Microstructure and shear rheology of entangled wormlike micelles in solution," J. Rheol. **53**, 441–458 (2009).
[36]M. E. Helgeson, M. D. Reichert, Y. T. Hu, and N. J. Wagner, "Relating shear banding, structure, and phase behavior in wormlike micellar solutions," Soft Matter **5**, 3858 (2009).
[37]J. C.-W. Lee, L. Porcar, and S. A. Rogers, "Unveiling temporal nonlinear structure–rheology relationships under dynamic shearing," Polymers **11**, 1189 (2019).
[38]B. Struth, K. Hyun, E. Kats, T. Meins, M. Walther, M. Wilhelm, and G. Grübel, "Observation of new states of liquid crystal 8CB under nonlinear shear conditions as observed via a novel and unique rheology/small-angle x-ray scattering combination," Langmuir **27**, 2880–2887 (2011).
[39]F. Westermeier, D. Pennicard, H. Hirsemann, U. H. Wagner, C. Rau, H. Graafsma, P. Schall, M. P. Lettinga, and B. Struth, "Connecting structure, dynamics and viscosity in sheared soft colloidal liquids: A medley of anisotropic fluctuations," Soft Matter **12**, 171–180 (2016).
[40]A. V. Zozulya, S. Bondarenko, A. Schavkan, F. Westermeier, G. Grübel, and M. Sprung, "Microfocusing transfocator for 1D and 2D compound refractive lenses," Opt. Express **20**, 18967 (2012).
[41]C. Rau, U. Wagner, Z. Pešić, and A. De Fanis, "Coherent imaging at the Diamond beamline I13," Phys. Status Solidi A **208**, 2522–2525 (2011).
[42]C. Rau, "Imaging with coherent synchrotron radiation: X-ray imaging and coherence beamline (I13) at diamond light source," Synchrotron Radiat. News **30**, 19–25 (2017).
[43]W. Bras, I. Dolbnya, D. Detollenaere, R. van Tol, M. Malfois, G. Greaves, A. Ryan, and E. Heeley, "Recent experiments on a small-angle/wide-angle x-ray scattering beam line at the ESRF," J. Appl. Crystallogr. **36**, 791–794 (2003).
[44]G. Portale, D. Cavallo, G. C. Alfonso, D. Hermida-Merino, M. van Drongelen, L. Balzano, G. W. M. Peters, J. G. P. Goossens, and W. Bras, "Polymer crystallization studies under processing-relevant conditions at the SAXS/WAXS DUBBLE beamline at the ESRF," J. Appl. Crystallogr. **46**, 1681–1689 (2013).
[45]D. Pennicard, S. Lange, S. Smoljanin, H. Hirsemann, H. Graafsma, M. Epple, M. Zuvic, M.-O. Lampert, T. Fritzsch, and M. Rothermund, "The LAMBDA photon-counting pixel detector," J. Phys.: Conf. Ser. **425**, 062010 (2013).
[46]D. Pennicard, S. Smoljanin, B. Struth, H. Hirsemann, A. Fauler, M. Fiederle, O. Tolbanov, A. Zarubin, A. Tyazhev, G. Shelkov, and H. Graafsma, "The LAMBDA photon-counting pixel detector and high-Z sensor development," J. Instrum. **9**, C12026 (2014).
[47]D. Kleshchanok, J.-M. Meijer, A. V. Petukhov, G. Portale, and H. N. W. Lekkerkerker, "Attractive glass formation in aqueous mixtures of colloidal gibbsite platelets and silica spheres," Soft Matter **7**, 2832 (2011).
[48]S. A. Rogers, "A sequence of physical processes determined and quantified in LAOS: An instantaneous local 2D/3D approach," J. Rheol. **56**, 1129 (2012).
[49]S. A. Rogers, "In search of physical meaning: Defining transient parameters for nonlinear viscoelasticity," Rheol. Acta **56**, 501–525 (2017).
[50]J. D. Park and S. A. Rogers, "The transient behavior of soft glassy materials far from equilibrium," J. Rheol. **62**, 869–888 (2018).
[51]J. D. Park and S. A. Rogers, "Rheological manifestation of microstructural change of colloidal gel under oscillatory shear flow," Phys. Fluids **32**, 063102 (2020).
[52]J. C.-W. Lee, K. M. Weigandt, E. G. Kelley, and S. A. Rogers, "Structure-property relationships via recovery rheology in viscoelastic materials," Phys. Rev. Lett. **122**, 248003 (2019).
[53]G. J. Donley, P. K. Singh, A. Shetty, and S. A. Rogers, "Elucidating the G″ overshoot in soft materials with a yield transition via a time-resolved experimental strain decomposition," Proc. Natl. Acad. Sci. U. S. A. **117**, 21945–21952 (2020).
[54]J. Choi, F. Nettesheim, and S. A. Rogers, "The unification of disparate rheological measures in oscillatory shearing," Phys. Fluids **31**, 073107 (2019).
[55]G. J. Donley, J. R. de Bruyn, G. H. McKinley, and S. A. Rogers, "Time-resolved dynamics of the yielding transition in soft materials," J. Non-Newtonian Fluid Mech. **264**, 117–134 (2019).
[56]G. J. Donley, W. W. Hyde, S. A. Rogers, and F. Nettesheim, "Yielding and recovery of conductive pastes for screen printing," Rheol. Acta **58**, 361–382 (2019).
[57]B. F. B. Silva, M. Zepeda-Rosales, N. Venkateswaran, B. J. Fletcher, L. G. Carter, T. Matsui, T. M. Weiss, J. Han, Y. Li, U. Olsson, and C. R. Safinya, "Nematic director reorientation at solid and liquid interfaces under flow: SAXS studies in a microfluidic device," Langmuir **31**, 4361–4371 (2015).
[58]C. R. Safinya, E. B. Sirota, R. F. Bruinsma, C. Jeppesen, R. J. Plano, and L. J. Wenzel, "Structure of membrane surfactant and liquid crystalline smectic lamellar phases under flow," Science **261**, 588–591 (1993).
[59]J.-C. P. Gabriel, F. Camerel, B. J. Lemaire, H. Desvaux, P. Davidson, and P. Batail, "Swollen liquid-crystalline lamellar phase based on extended solid-like sheets," Nature **413**, 504–508 (2001).
[60]S. H. L. Klapp and S. Hess, "Shear-stress-controlled dynamics of nematic complex fluids," Phys. Rev. E **81**, 051711 (2010).
[61]Y. Méheust, K. D. Knudsen, and J. O. Fossum, "Inferring orientation distributions in anisotropic powders of nano-layered crystallites from a single two-dimensional WAXS image," J. Appl. Crystallogr. **39**, 661–670 (2006).
[62]F. D. Giudice, B. V. Cunning, R. S. Ruoff, and A. Q. Shen, "Filling the gap between transient and steady shear rheology of aqueous graphene oxide dispersions," Rheol. Acta **57**, 293–306 (2018).